KKU SCIENCE JOURNAL
Journal Home Page : https://ph01.tci-thaijo.org/index.php/KKUSciJ
Published by the Faculty of Science, Khon Kaen University, Thailand

วิถีการโคจรของอนุภาคแบบมีมวลรอบวัตถุหนาแน่นที่มีประจุแม่เหล็กภายใต้สนามโน้มถ่วงแบบไอน์สไตน์-แม็กซ์เวลล์-ดีเลตรอน

Trajectory of Massive Particle Around a Magnetically Charged Compact Object in Einstein-Maxwell-dilaton Gravity

ชวิศ ศักกะวัฒนา[1] และ สุภัคชัย พงศ์เลิศสกุล[1*]

Chawit Sakkawattana[1] and Supakchai Ponglertsakul[1*]

[1]กลุ่มวิจัยฟิสิกส์ทฤษฎี Strong gravity ภาควิชาฟิสิกส์ คณะวิทยาศาสตร์ มหาวิทยาลัยศิลปากร จังหวัดนครปฐม 73000

[1]Strong Gravity Group, Department of Physics, Faculty of Science, Silpakorn University, Nakhon Pathom, 73000, Thailand

บทคัดย่อ

ในงานวิจัยนี้ เราศึกษาการเคลื่อนที่แบบวงโคจรของอนุภาคที่มีมวลรอบวัตถุหนาแน่นที่มีประจุแม่เหล็ก ซึ่งอยู่ในสภาวะนิ่งและมีสมมาตรทรงกลม ภายใต้สนามโน้มถ่วงแบบไอน์สไตน์-แม็กซ์เวลล์-ดีเลตรอน ผลที่ได้วิเคราะห์นี้มีตัวแปรลักษณะเฉพาะสามตัว ได้แก่ ฟลักซ์ของดีเลตรอน ประจุแม่เหล็ก และค่าคงที่ของดีเลตรอน ผลลัพธ์เหล่านี้ช่วยให้สามารถเข้าใจพฤติกรรมทางกายภาพของวัตถุที่มีประจุแม่เหล็กในทฤษฎีสัมพัทธภาพทั่วไปได้จากการสังเกตการณ์

ABSTRACT

In this work, we investigate an orbital motion of massive particle around a static and spherically symmetric magnetically charged object in Einstein-Maxwell-dilaton gravity. This solution has three characteristics parameters, dilaton flux D, magnetic charged P and dilaton coupling constant λ. These results provide observational means for understanding physical behaviors of magnetically charged compact object in general relativity.

คำสำคัญ: วิถีการโคจร อนุภาคแบบมีมวล สนามโน้มถ่วงแบบไอน์สไตน์-แม็กซ์เวลล์-ดีเลตรอน

Keywords: Trajectory, Massive Particle, Einstein-Maxwell-dilaton (EMD)

INTRODUCTION

The motion of test particles around compact astrophysical objects serves as a powerful tool to probe the nature of spacetime geometry and to test alternative theories of gravity in the strong-field regime. Among the extended theories motivated by string theory and low-energy effective actions, Einstein-Maxwell-dilaton (EMD) gravity introduces a scalar dilaton field that couples to both the gravitational and

*Corresponding Author, E-mail: ponglertsakul_s@silpakorn.edu

Received date: 7 May 2025 | Revised date: 15 October 2025 | Accepted date: 22 October 2025

doi: 10.14456/kkuscij.2026.6

electromagnetic sectors, resulting in significant modifications to black hole and compact object solutions compared to general relativity (GR) (Gibbons and Maeda, 1988; Garfinkle *et al.,* 1991). For example, in (Promsiri *et al*., 2023), the shadow of electrically charged black hole in the EMD theory is investigated. In GR, the photon ring radius of the Schwarzschild black hole $(3\mathrm{M})$, where M is the Schwarzschild black hole mass, is the largest. The authors of (Promsiri *et al.,* 2023) find that the presence of dilaton coupling leads to a possibility that photon ring radius can be larger than $3\mathrm{M}$.

In particular, EMD gravity allows the existence of magnetically charged black holes, which are of special interest due to their unique spacetime structures and their role in our understanding of the interactions between scalar, electromagnetic, and gravitational fields. Unlike their electrically charged counterparts, magnetically charged solutions are often less explored, especially in relation to geodesic motion and observational consequences such as gravitational lensing, particle acceleration, and accretion phenomena (Hirschmann *et al.,* 2018).

Analyzing the trajectories of massive particles in such spacetimes can offer insights into the influence of the dilaton field and magnetic charge on the stability and characteristics of orbits. This becomes especially relevant in regimes where deviations from general relativity may be non-negligible. Prior works have considered test particle motion around dilatonic black holes (Minazzoli and Wavasseur, 2025; Vargas and Cuyubamba, 2024), but few have examined in depth the combined effects of magnetic charge and dilaton coupling on massive particle dynamics.

In addition to studying of how massive particles move in curved spacetime, it is also interesting to explore how photon behaves close to black holes. For instance, shadows of Kerr black hole with scalar hair presents a novel shape and smaller in size (Porfyriadis and Remmen, 2023) compared to the shadow of standard Kerr black hole. Moreover, null geodesics of black hole in the EMD theory is explored in (Promsiri *et al*., 2023) where an influence of black hole electric charge and dilaton coupling constant on null geodesics are studied. The width of photon ring depends on black hole's electric charge and the coupling constant.

In this paper, we investigate the motion of massive particles around a magnetically charged compact object in Einstein-Maxwell-dilaton gravity. We derive the equations of motion, analyze the effective potential, and classify the types of orbits-tracing stable circular, bound, and escape trajectories. The results may provide both theoretical insights and observational signatures to identify non-standard compact objects in astrophysical settings.

Magnetically charged object on Einstein-Maxwell-dilaton gravity

In this section, we introduce a spherically symmetric static general solution from EMD gravity. The EMD action is given by (Garfinkle *et al*., 1991)

$$S_{EMD} = \int d^4x\sqrt{-g_E}\left(\mathcal{R} - 2g_E^{\mu\nu}\nabla_\mu\Phi\nabla_\nu\Phi - f(\Phi)F_{\mu\nu}F^{\mu\nu}\right), \tag{1}$$

where the coupling function of Maxwell and dilaton field is $f(\Phi) = e^{-2\lambda\Phi}$, λ is the dilaton coupling constant. When g_E is the determinant of metric tensor $g_{\mu\nu}$ in Einstein's frame relativity, $\mathcal{R}$ is the

Ricci tensor, $g_E^{\mu\nu}$ is the inverse of metric tensor in Einstein's frame, Φ is the dilaton field, $F_{\mu\nu}$ and $F^{\mu\nu}$ is the Maxwell tensor and its inverse, respectively. The Maxwell tensor $F_{\mu\nu}$ in purely magnetic case has only an angular component (θ, ϕ) and the dilaton profile are given by (Porfyriadis and Remmen, 2023)

$$F = P \sin\theta \, d\theta \wedge d\phi. \tag{2}$$

$$\Phi(r) = -\frac{\lambda}{2(1+\lambda^2)} log\left[\frac{(r-r_+)(r-r_-)}{r^2}\right] \pm \frac{\lambda\Delta}{2} log\left[\frac{r-r_+}{r-r_-}\right] + \Phi_0. \tag{3}$$

where we set $\Phi_0 = 0$ without loss of generality. The spherically symmetric static line element solution is

$$ds^2 = -f(r)dt^2 + g(r)dr^2 + h(r)(d\theta^2 + Sin^2\theta d\phi^2\,). \tag{4}$$

The metric functions are given by

$$f(r) = \left(\frac{r-r_+}{r-r_-}\right)^{\pm\Delta}\left(\frac{(r-r_-)(r-r_+)}{r^2}\right)^{\frac{1}{1+\lambda^2}}, \tag{5}$$

$$g(r) = \left(\frac{r-r_+}{r-r_-}\right)^{\frac{2}{q}\mp\Delta}\left(\frac{(r-r_-)(r-r_+)}{r^2}\right)^{\frac{\lambda^2}{1+\lambda^2}}\left(\frac{r_\pm r_-}{q}\right)^4\left(\frac{\Pi(r)^{-4}r^2}{(r-r_+)^3(r-r_-)^3}\right), \tag{6}$$

$$h(r) = \left(\frac{r-r_+}{r-r_-}\right)^{-1+\frac{1}{q}\mp\Delta}\left(\frac{r(r_+-r_-)}{q(r-r_-)\Pi(r)}\right)^2. \tag{7}$$

where we define $\Delta \equiv \frac{\lambda\sqrt{1-q^2+\lambda^2}}{q(1+\lambda^2)}$, $\Pi(r) \equiv \left(\frac{r-r_+}{r-r_-}\right)^{\frac{1}{q}} - 1$ with r_+ and r_- being the outer and inner horizons, respectively. We introduce a parameter q that represents a relation to Komar mass ($\widetilde{M}$), magnetic charged ($\tilde{P}$), and integrated dilaton flux ($\widetilde{D}$). These are given by

$$\widetilde{M} = \frac{r_+ + r_-}{2(1+\lambda^2)} + \frac{\lambda(r_+ - r_-)}{2(1+\lambda^2)}\frac{\sqrt{1-q^2+\lambda^2}}{q}, \tag{8}$$

$$\tilde{P} = \sqrt{\frac{2r_+r_-}{1+\lambda^2}}, \tag{9}$$

$$\widetilde{D} = -\frac{\lambda(r_+ + r_-)}{2(1+\lambda^2)} + \frac{r_+ - r_-}{2(1+\lambda^2)}\frac{\sqrt{1-q^2+\lambda^2}}{q}. \tag{10}$$

These parameters are global charges defined by the Kormar formula given in (Porfyriadis and Remmen, 2023). In a similar manner as finding total electric charged by integrating the electric field over a certain surface, these charges are the source of the corresponding fields i.e., $\widetilde{M}$ as source of gravitational field, $\tilde{P}$ as source of electromagnetic field and $\widetilde{D}$ as source of scalar field. In this case, the fields are integrated over the surface at spatial infinity. To reduce the magnetic charged $\tilde{P}$ and dilaton flux $\widetilde{D}$ parameters into a simple form. We define the following parameters

$$P = \frac{\tilde{P}}{\sqrt{2\widetilde{M}}}, \text{ and } D = \frac{\widetilde{D}}{\widetilde{M}}. \tag{11}$$

Then, we can write parameter q as

$$q^2 = \frac{(1-\lambda D)^2 - (1+\lambda^2)P^2}{1+D^2-P^2}. \tag{12}$$

From eq. (8) - (11), the horizon can be derived as

$$r_+ = 1 - \lambda D \pm \sqrt{(1-\lambda D)^2 - (1+\lambda^2)P^2}, \tag{13}$$

$$r_- = \frac{(1+\lambda^2)P^2}{1-\lambda D \pm \sqrt{(1-\lambda D)^2 - (1+\lambda^2)P^2}} \tag{14}$$

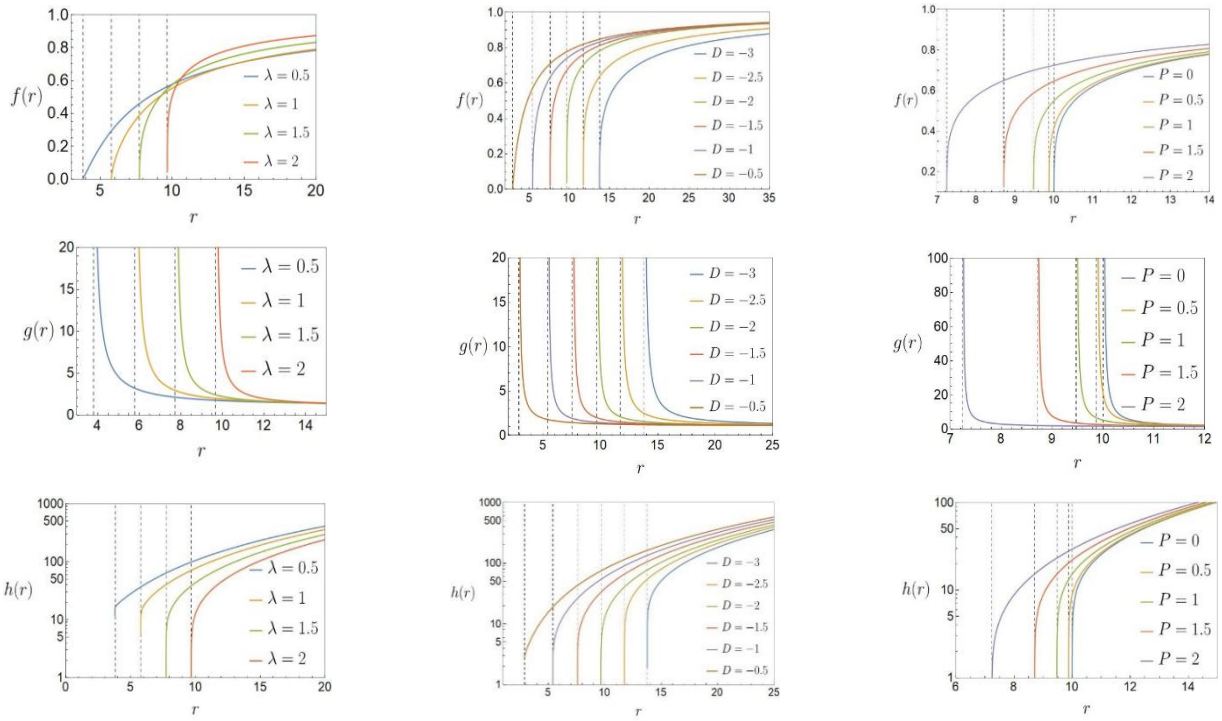

Figure 1 shows the behavior of the metric functions $f(r), g(r)$, and $h(r)$ as a function of the radius from top to bottom row respectively, with the variation of the parameters λ, D, and P shown from left column to right column, respectively. In the first column, there are the variations of λ for fixed $D = -2$ and $P = 0.8$. In the second column, there are the variations of D with fixed $\lambda = 2$ and $P = 0.8$. In right column, there are the variations of P with fixed $\lambda = 2$ and $D = -2$. The plots indicate that the metric function asymptotically approaches flatness at large radii.

Time-like geodesics

In this section, we consider time-like geodesics of EMD charged compact object. To analyze the geodesics, we use Hamilton-Jacobi equation method (Chandrasekhar, 1998), from eq. (4) the Lagrangian is

$$\mathcal{L} = \frac{1}{2} g_{\mu\nu} \dot{x}^\mu \dot{x}^\nu = \frac{1}{2}\left[-f(r)\dot{t}^2 + g(r)\dot{r}^2 + h(r)\left(\dot{\theta}^2 + Sin^2\theta\dot{\phi}^2\right)\right]. \tag{15}$$

The canonical momenta can be calculated by $p_\mu = \frac{\partial \mathcal{L}}{\partial \dot{x}^\mu} = g_{\mu\nu}\dot{x}^\nu$,

$$p_t = -f(r)\dot{t}, \tag{16}$$

$$p_r = g(r)\dot{r}, \tag{17}$$

$$p_\theta = h(r)\dot{\theta}, \tag{18}$$

$$p_\phi = h(r)sin^2\theta\dot{\phi}\,. \tag{19}$$

From Hamilton-Jacobi equation, $\frac{\partial S}{\partial x^\mu} = p_\mu$ and $S = \int \mathcal{L}\, d\lambda$. Therefore, we obtain

$$\frac{\partial S}{\partial \lambda} = -\frac{1}{2} g^{\mu\nu} p_\mu p_\nu \tag{20}$$

The Jacobi action S can be separated into $S = \frac{1}{2}\delta\lambda - Et + L\phi + S_r(r) + S_\theta(\theta)$ where the constant E is energy, and the constant L is angular momentum. The separation of Jacobi action above is found by Carter (Carter, 1968) where the given form makes the Hamilton-Jacobi equation solvable. For null- or time-like geodesics, we have $\delta = 0$ or 1. Thus, we get

then
$$\frac{1}{2}\delta = -\frac{1}{2}\left[-\frac{E^2}{f(r)} + \frac{1}{g(r)}\left(\frac{\partial S_r}{\partial r}\right)^2 + \frac{1}{h(r)}\left(\frac{\partial S_\theta}{\partial \theta}\right)^2 + \frac{L^2}{h(r)sin^2\theta}\right], \tag{21}$$

$$h(r)\delta - \frac{h(r)}{f(r)}E^2 + \frac{h(r)}{g(r)}\left(\frac{\partial S_r}{\partial r}\right)^2 + L^2 = -\left(\frac{\partial S_\theta}{\partial \theta}\right)^2 - L^2 cot^2\theta\,. \tag{22}$$

The left-hand side (LHS) of eq. (22) depends on radial coordinate and the right-hand side (RHS) solely depends on the angular coordinate. Therefore, we can equate both side of eq. (22) to a constant $-\mathcal{Q}$.

$$LHS = RHS = -\mathcal{Q}\,,$$

where $\mathcal{Q}$ is carter constant. Since, we have

$$\mathcal{R}(r) = \frac{h^2(r)f(r)}{g(r)}\left(\frac{\partial S_r}{\partial r}\right)^2, \tag{23}$$

$$\Theta(\theta) = \left(\frac{\partial S_\theta}{\partial \theta}\right)^2. \tag{24}$$

Then, these are

$$\mathcal{R}(r) = h^2(r)E^2 - f(r)h(r)[h(r)\delta + L^2 + \mathcal{Q}], \tag{25}$$

$$\theta(\theta) = \mathcal{Q} - L^2 cot^2\theta\,. \tag{26}$$

From eq. (16) - (19), we get

$$\left(\frac{dr}{d\lambda}\right) = \frac{1}{h(r)}\sqrt{\frac{\mathcal{R}(r)}{f(r)g(r)}}, \tag{27}$$

$$\left(\frac{d\theta}{d\lambda}\right) = \frac{1}{h(r)}\sqrt{\Theta(\theta)}\,. \tag{28}$$

The radial equation of motion of particle is

$$\left(\frac{dr}{d\lambda}\right)^2 + \tilde{V}_{eff}(r) = E^2. \tag{29}$$

From eq. (25) and (27), the effective potential is

$$\tilde{V}_{eff}(r) = E^2\left(1 - \frac{1}{f(r)g(r)}\right) + \frac{1}{g(r)h(r)}[h(r)\delta + L^2 + \mathcal{Q}].$$

The radial equation above explain how photon propagates under the influence of gravitational potential $\tilde{V}_{eff}(r)$. In this work, we consider the orbital motion of massive particle on the equatorial plane, that is $\theta = \frac{\pi}{2}$ and $\dot{\theta} = 0$. Eq. (22) leads to $\mathcal{Q} = 0$. After that, we redefine a parameter of eq. (29) under $\lambda = \frac{\tilde{\lambda}}{|L|}$, which can be rewritten as

$$\left(\frac{dr}{d\tilde{\lambda}}\right)^2 + V_{eff}(r) = \frac{1}{b^2}, \tag{30}$$

where $b = \frac{|L|}{E}$ and $V_{eff} = \tilde{V}_{eff}|_{\mathcal{Q}=0,\delta=1}$. In this work, we consider time-like geodesics, which means $\delta = 1$. Hence, the effective potential for time-like curved on the equatorial plane takes the form

$$V_{eff} = \frac{1}{b^2}\left(1 - \frac{1}{f(r)g(r)}\right) + \frac{1}{g(r)}\left(1 + \frac{1}{h(r)}\right). \tag{31}$$

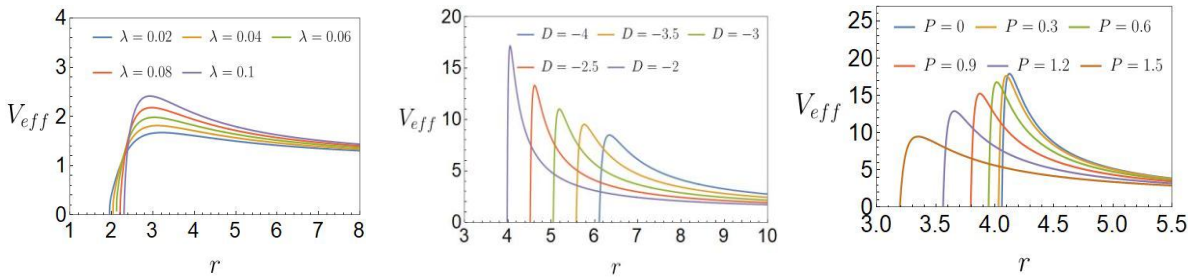

Figure 2 The effective potential V_{eff} for different value of parameters. In left panel we fix parameters $D = -2, P = 0.5, \lambda = 10$. In the middle panel, we fix $\lambda = 0.5, P = 0.5$. In the right panel, we fix $\lambda = 0.5, D = -2$. Note that in this figure, the impact parameter is fixed to 10.

Now let us consider the innermost stable circular orbit (ISCO). ISCO plays a crucial role in characterizing the dynamics of particles in strong gravitational fields, as it marks the transition between stable and unstable circular trajectories (Chandrasekhar, 1998; Yagi and Stein, 2016). For a time-like geodesic, the conditions for circular motion are obtained by requiring the effective potential $V_{eff}(r)$ to satisfy

$$V'_{eff} = 0, V''_{eff} = 0. \tag{32}$$

From the above condition, we can be obtaining the radius of ISCO r_{ISCO}, which corresponds to parameters $\lambda, D,$ and P. To understand the orbital motion of particle, the standard approach is to observe the motion in $r - \phi$ plane. To achieve this, let us consider the following

$$\left(\frac{dr}{d\phi}\right)^2 = \left(\frac{dr}{d\tilde{\lambda}}\right)^2\left(\frac{d\tilde{\lambda}}{d\phi}\right)^2 = \frac{h^2(r)}{g(r)}\left[\frac{1}{b^2 f(r)} - \frac{1}{h(r)} - \frac{1}{L^2}\right]. \tag{33}$$

By introducing $u \equiv \frac{1}{r}$, we have u as a function of ϕ, $u(\phi)$. Therefore, the radial equation is now

$$\left(\frac{du}{d\phi}\right)^2 = u^4 \frac{h\left(\frac{1}{u}\right)^2}{g\left(\frac{1}{u}\right)}\left[\frac{1}{b^2 f\left(\frac{1}{u}\right)} - \frac{1}{h\left(\frac{1}{u}\right)} - \frac{1}{L^2}\right] \equiv P(u). \tag{34}$$

As a final step, we differentiate the above equation with respect to ϕ. We arrive at the standard second-order differential equation

$$\frac{d^2u(\phi)}{d\phi^2} = \frac{1}{2}\frac{dP}{d\phi}, \tag{35}$$

It can be solved by standard differential equation solver programing. In practice, we initially set the starting point (p) of a particle at $u(0) = \frac{1}{p}$ and demand that $\frac{du}{d\phi} = 0$ at $\phi \to 0$ which serves as our initial condition when integrating eq. (34). The resulting $u(\phi)$ explains how a massive particle moves around the compact object in the EMD gravity.

The analysis of the behavior of the effective potential V_{eff} of EMD charged compact object surrounded by massive particles are shown in Fig.2. In left panel, we vary parameter λ and fix parameter $D = -2$ $P = 0.5$ and $b = 10$. We find that when λ increases, the peak of the effective potential tends to get higher, and all the variations approaches a constant when r increases. The location of the minimum of the potential (when it exists) shifts to the right with increasing λ, suggesting a larger stable circular orbit radius. The middle panel illustrates how V_{eff} changes with r for various values of the parameter P, from $P = 0$ to $P = 1.5$ and fixed $D = -2, \lambda = 0.5$ and $b = 10$. As P increases, the peak of the potential becomes sharper and shifts to the right. The maximum value of V_{eff} also increases with P, suggesting a higher potential barrier and the potential well becoming narrower and more localized with higher P. The growing barrier and its shifting position suggest that increasing P makes it harder for a particle to approach the central region, potentially affecting the stability and radius of circular orbits. The right panel of fig .2 displays the effective potential as a function of r for different values of D, ranging from $D = -4$ to $D = -2$ with fixed $\lambda = 0.5,\ P = 0.5$ and $b = 10$. As D increases (becomes less negative), The peak of the effective potential shifts to larger r and decreases in magnitude, and the potential well becomes wider and shallower with increasing D.

Next, we will consider a trajectory of massive particle around EMD charged compact object from a top-view as shown in Fig. 3. The first row shows the variation of $\lambda = 0.3, 0.8,$ and 1.3 with fixed parameters $D = -1$ and $P = 0.5$. We find that when λ increases, the compact object and the orbital radius get bigger. The orbital path has a gradual change in course and appears more orderly. The second row shows the variation of $D = -1.5,\ -1,$ and $-0.5.$ with fixed $\lambda = 1.5$ and $P = 0.1.$ The size of compact object decreases with increasing D while the orbital radius of massive particle gets wider. The last row shows the variation of parameter $P = 0.5, 1,$ and $P_{max}(1.25219)$ with fixed $\lambda = 0.5$ and $D = -0.8$. To compare with the general relativity, we plot trajectories of massive particle around the magnetically charged Reissner-Nordstrom (RN) black hole in the left and the middle panels of the last row figures. The trajectories are denoted by red solid curves and the corresponding ISCO are shown

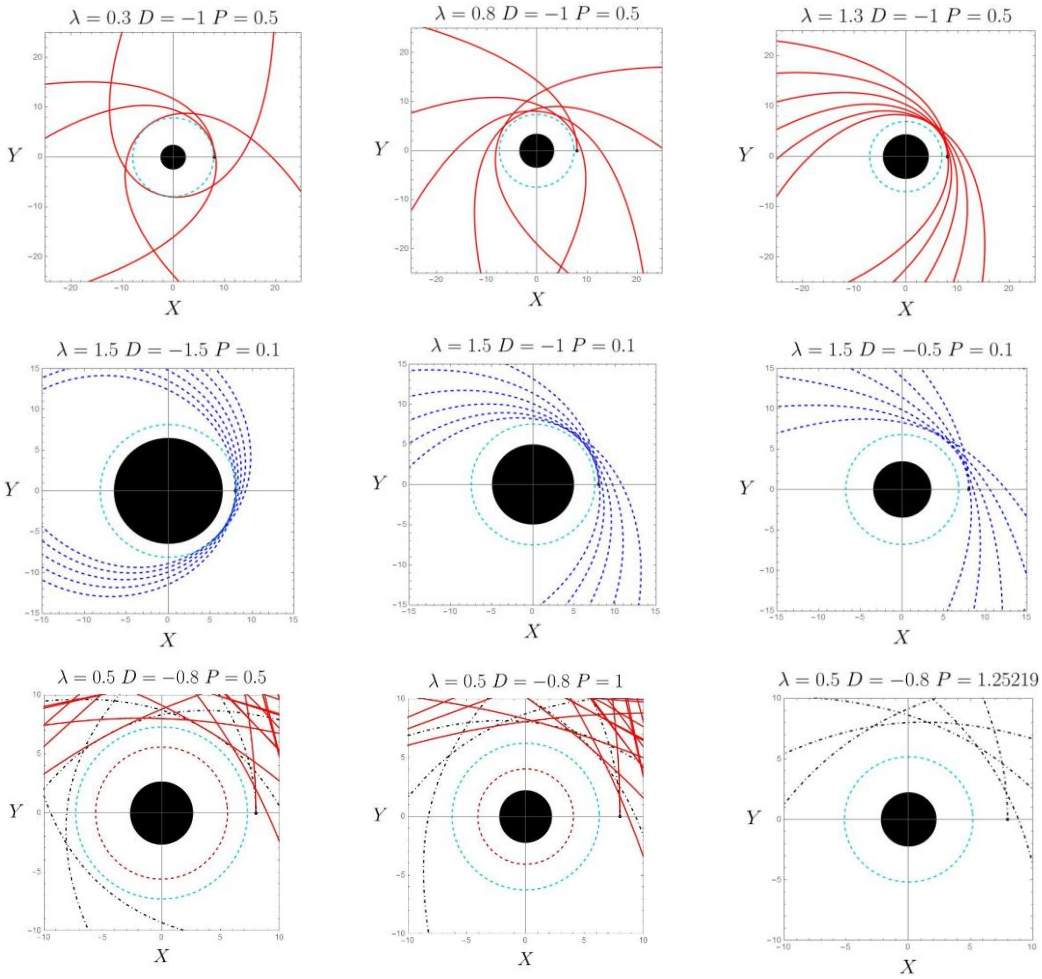

Figure 3 The trajectory of massive particle around EMD charged compact object for different values of $\lambda, D,$ and P The initial position of massive particle is at $(8,0)$ in coordinate $X-Y.$ The black disk at the center denotes a compact object where the blue dotted circle is the innermost stable circular orbit (ISCO). In the first row, λ is varied for $\lambda = 0.3, 0.8,$ and 1.3 with fix $D = -1$ and $P = 0.5.$ The second row, D is varied for $D = -1.5, -1,$ and -0.5 with fixed $\lambda = 1.5$ and $P = 0.1$. The last row is the variation of P for $P = 0.5,1,$ and $P_{max}(1.25219)$ with fixed $\lambda = 0.5$ and $D = -0.8$. We set impact parameter $b = 5$ and $L = 4.25$. In the left and middle panel of the last row, the trajectories of massive particle around the Reissner-Nordstrom are represented by red curves where the red dotted curve represents ISCO corresponding to the Reissner-Nordstorm case. as a red dotted circle. Remark that for the RN case, $P > 1$ yields a naked singularity scenario, which is out of scope of our study. Here, we observe that ISCO of the RN solution in GR is generally smaller than the compact solution in the EMD gravity. Moreover, the orbits close to the central object appear to be more chaotic in GR than in the EMD gravity. The size of the object decreases when P increases whereas the orbital radius gets wider. These findings highlight the roles of the parameters λ, D, and P in shaping the gravitational field and influencing the dynamical motion of particles around the compact object. This provides valuable insight for further analysis within the EMD theoretical framework.

CONCLUSIONS

In this study, we have investigated the orbital motion of massive particles in the gravitational field of a magnetically charged compact object within the framework of Einstein-Maxwell-dilaton (EMD) gravity. By deriving the geodesic equations, using the Hamilton-Jacobi formalism and analyzing the effective potential, we have shown that the presence of a dilaton field and magnetic charge significantly alters the dynamics compared to standard general relativistic scenarios.

Our results indicate that the effective potential is highly sensitive to the values of the dilaton coupling constant λ, the magnetic charge P, and the integrated dilaton flux D. Specifically, increasing λ or D tends to shift the location of the innermost stable circular orbit (ISCO) outward and reduce the depth of the potential well. This is consistent with results from scalar-tensor gravity models, which often predict weakened gravitational attraction due to scalar field screening effects (Cunha *et al*., 2015). Such behavior has also been discussed in dilaton black hole models in higher-dimensional or string-inspired gravity theories, where modified orbital characteristics have been proposed as potential observational signatures of new physics beyond general relativity (Sotiriou and Faraoni, 2008; Fernando, 2006; Chen, 2019).

Moreover, the impact of the magnetic charge on particle trajectories reveals a rich structure in the effective potential landscape, contributing to a deeper understanding of the interplay between electromagnetic and scalar interactions in curved spacetime. This aligns with findings in studies of nonlinear electrodynamics coupled to scalar fields, which have similarly demonstrated modifications to particle motion and black hole properties (Ayón-Beato and García, 1998).

The qualitative behavior of orbits such as the transition from bound to unbound trajectories and the sensitivity of ISCO radii to model parameters highlights the potential for distinguishing EMD compact objects from classical black holes through astrophysical observations. These findings are particularly relevant in light of recent developments in black hole imaging, gravitational wave astronomy, and precision timing of pulsars near compact objects, all of which offer promising avenues to test deviations from general relativity in the strong-field regime (Yagi and Stein, 2016; Moffat and Toth, 2020).

For future work, it would be valuable to extend the present analysis to include rotation (i.e., axisymmetric EMD spacetimes), study the influence of a cosmological constant, and examine the role of massive scalar fields or higher-order curvature corrections. Such extensions may further enhance our understanding of how dilaton and magnetic effects can influence astrophysical processes and provide unique observational footprints.

REFERENCES

Ayón-Beato, E. and García, A. (1998). Regular black hole in general relativity coupled to nonlinear electrodynamics. Physical Review Letters 80(23): 5056 - 5059 doi: 10.1103/physrevlett.80.5056.

Carter, B. (1968). Hamilton-Jacobi and Schrödinger separable solutions of Einstein's equations. Communications in Mathematical Physics 10(4): 280 - 310. doi: 10.1007/BF03399503.

Chandrasekhar, S. (1998). The Mathematical Theory of Black Holes. (1st ed). New York: Oxford University Press.

Chen, C.Y., Bouhmadi-López, M. and Chen, P. (2019). Probing Palatini-type gravity theories through gravitational wave detections via quasi-normal modes. The European Physical Journal C 79: 63. doi: 10.1140/epjc/s10052-019-6585-y.

Cunha, P.V.P., Herdeiro, C.A.R., Radu, E. and Rúnarsson, H.F. (2015). Shadows of Kerr Black Holes with Scalar Hair. Physical Review Letters 115(21): 211102. doi: 10.1103/physrevlett.115.211102.

Fernando, S. (2006). Thermodynamics of Born-Infeld–anti-De Sitter black holes in the grand canonical ensemble. Physical Review D 74(10): 104032. doi: 10.1103/physrevd.74.104032.

Garfinkle, D., Horowitz, G.T. and Strominger, A. (1991). Charged black holes in string theory. Physical Review D 43(10): 3140 - 3143. doi: 10.1103/physrevd.43.3140.

Gibbons, G.W. and Maeda, K.I. (1988). Black holes and membranes in higher-dimensional theories with dilaton fields. Nuclear Physics B 298(4): 741 - 775. doi: 10.1016/0550-3213(88)90006-5.

Hirschmann, E. W., Lehner, L., Liebling, S.L. and Palenzuela, C. (2018). Black hole dynamics in Einstein-Maxwell-Dilaton theory. Physical Review D 97(6): 064032. doi: 10.1103/physrevd.97.064032.

Minazzoli, O. and Wavasseur, M. (2025). Compact objects with scalar charge imbedded in a magnetic or electric field in Einstein-Maxwell-dilaton theories. The European Physical Journal C 85(4): 474. doi: 10.1140/epjc/s10052-025-14179-w.

Moffat, J.W. and Toth, V.T. (2020). Masses and shadows of the black holes Sagittarius A* and M87* in modified gravity. Physical Review D 101(2): 024014. doi: 10.1103/physrevd.101.024014.

Porfyriadis, A.P. and Remmen, G.N. (2023). Charged dilatonic spacetimes in string theory. Journal of High Energy Physics 2023(3): 125. doi: 10.1007/jhep03(2023)125.

Promsiri, C., Horinouchi, W. and Hirunsirisawat, E. (2023). Remarks on the light ring images and the optical appearance of hairy black holes in Einstein-Maxwell-dilaton gravity. The European Physical Journal C 84(9): 910. doi: 10.1140/epjc/s10052-024-13258-8.

Sotiriou, T.P. and Faraoni, V. (2008). f(R) theories of gravity. Reviews of Modern Physics 82(1): 451 - 497. doi: 10.1103/revmodphys.82.451.

Vargas, R.M. and Cuyubamba, M.A. (2024). Motion of test particles around an Einstein-Dilaton-Gauss–Bonnet black hole in a uniform magnetic field. Annals of Physics 473: 169907. doi: 10.1016/j.aop.2024.169907.

Yagi, K. and Stein, L. C. (2016). Black hole based tests of general relativity. Classical and Quantum Gravity 33(5): 054001 doi: 10.1088/0264-9381/33/5/054001.

❑❑❑❑❑